The 2011 Nabro eruption, a SO$_2$ plume height analysis using IASI measurements

L. Clarisse[1], **P.-F. Coheur**[1], **N. Theys**[2], **D. Hurtmans**[1], and **C. Clerbaux**[1,3]

[1]Spectroscopie de l'Atmosphère, Service de Chimie Quantique et Photophysique, Université Libre de Bruxelles, Brussels, Belgium
[2]Belgian Institute for Space Aeronomy, Brussels, Belgium
[3]UPMC Univ. Paris 6; Université Versailles St.-Quentin; CNRS/INSU, LATMOS-IPSL, Paris, France

Correspondence to: L. Clarisse (lclariss@ulb.ac.be)

Abstract. In the wake of the June 2011 Nabro eruption, large stratospheric plumes were observed by several instruments up to altitudes of 21 km, much higher than initial reported injection heights. It has been debated whether deep convection associated with the Asian Summer Monsoon anticyclone played a vital role in the vertical transport of the plume. Here we present a new and fast SO$_2$ height retrieval algorithm for observations of the Infrared Atmospheric Sounding Interferometer (IASI). A comprehensive validation with forward trajectories and coincident CALIOP measurements is presented which indicates an accuracy better than 2 km for plumes below 20 km and SO$_2$ columns up to the 1 DU level. We use this new product to analyse the Nabro eruption. Our findings indicate an initial plume located mainly between 15 and 17 km for which the lower parts underwent in succession rapid descent and uplift, within the Asian Monsoon anticyclone circulation, up to the stable thermal tropopause between 16 and 18 km, from where it slowly ascended further into the stratosphere. Evidence is presented that emissions in the first week of the eruption also contributed to the stratospheric sulfur input. This includes a second eruption between 15 and 17 km on the 16th and continuous emissions in the mid-troposphere of which some were also entrained and lifted within the anticyclonic circulation.

1 Introduction

Nabro is a volcano located in the Afar Depression in Eritrea, near the Ethiopian border at 13.37° N, 41.70° E with a summit elevation of 2218 m a.s.l. The volcano was classified as inactive, with no known eruption in the past 10 000 yr (Bojanowski, 2011) until it started erupting violently on 12 June 2011. The SEVIRI instrument on board the Meteosat-9 platform was the first to observe the volcanic plume around 20:30 UTC (Pavolonis, 2012). This initial plume was observed later by many other satellite instruments and was found to be very rich in water vapour and sulphur dioxide (SO$_2$) but relatively poor in mineral ash (Clarisse et al., 2012). Nabro kept on erupting almost continuously for one month to follow (SACS, 2013), but with decreasing intensity, both in terms of injection height and SO$_2$ flux (Theys et al., 2013).

In the first phase of the eruption, the main transport pattern of emitted SO$_2$ followed the strong anticyclonic circulation over the Middle East and Asia associated with the Asian summer monsoon at that time of year, indicative of upper tropospheric–lower stratospheric (UTLS) heights (Clarisse et al., 2012; Sawamura et al., 2012; Bourassa et al., 2012; Bergman et al., 2012). At these heights a major atmospheric sink for SO$_2$ is oxidation, leading to the formation of hydrated sulfuric acid droplets. Such aerosols were observed building up in the Northern Hemispheric stratosphere in increasingly large loadings in the wake of the eruption. The OSIRIS/Odin limb sounder for instance measured its largest aerosol load since it was launched in 2001 (Bourassa et al.,

2012). Other instruments that witnessed this process include the CALIOP/CALIPSO lidar (Sawamura et al., 2012; Bourassa et al., 2012; Vernier et al., 2013), a network of ground-based lidars (Sawamura et al., 2012; Uchino et al., 2012) and a CCD camera (Mateshvili et al., 2013). In the first month after the eruption stratospheric aerosols were mainly observed over Asia and the Middle East; by day 60 they covered the whole Northern Hemisphere. Reported aerosol altitudes from these instruments are between 15 and 21 km.

Sulfate aerosols in the stratosphere have a residence time of the order of months to years and can have important impacts on local and global climate. The most important direct effect is scattering of solar radiation, which leads to cooling of surface temperatures (e.g. Stenchikov et al., 1998; Robock, 2000). A more indirect effect includes the impact of sulphate aerosols on precipitation, in particular due to weakening of the Asian and African summer monsoons (Trenberth and Dai, 2007; Robock et al., 2007). Since the year 2000, the background stratospheric aerosol load has increased substantially (Hofmann et al., 2009), yielding a negative forcing of $-0.1\,\mathrm{W\,m^{-2}}$ and partially offsetting the radiative forcing of greenhouse gases (Solomon et al., 2011). This increase is likely due to a series of small to medium sized volcanic eruptions injecting SO_2 in the lower stratosphere at tropical latitudes (Vernier et al., 2011a, b). To understand present day climate and how it might change, it is therefore vital to identify and quantify (potential) injection and transport patterns of SO_2 and sulphate aerosol in the stratosphere. Of particular interest are tropical volcanic eruptions, which have potentially the largest impact on the climate.

The recent eruption of Nabro constitutes a fascinating case study in this perspective, especially as it is debated whether the volcanic plume was directly injected in the stratosphere or whether it was brought to these altitudes by (convective) transport. We refer to the original report (Bourassa et al., 2012) and comments (Fromm et al., 2013; Vernier et al., 2013; Bourassa et al., 2013) for a full account and only summarise the main points here. Bourassa et al. (2012) argue that the Asian Monsoon is responsible for the relatively rapid ascent of the tropospheric Nabro plume in the stratosphere. They adopt tropospheric injection heights (10–13 km) based on a report of the Toulouse VAAC, a CALIOP image on 16 June and consistency of the observed transport pattern with NCEP winds at these heights. Measurements using the OSIRIS and CALIOP sounder reveal stratospheric aerosols building up above the Asian Monsoon region, and residing there for a long time before spreading to the rest of the Northern Hemisphere. The anticyclonic circulation of the Asian summer monsoon is known to trap air masses within the UTLS. On its eastern side it contains a deep convective region, which can transport tropospheric air to the (lower) stratosphere and confine it within (Li et al., 2005; Randel and Park, 2006; Park et al., 2007, 2008, 2009; Randel et al., 2010). Calipso's overpasses on 1 July over this region show aerosol layers mainly between 16–19 km and over high

altitude convective clouds located between 12–16 km. These facts together with the satellite observations allow Bourassa et al. (2012) to reach their conclusion on the role of the Asian Monsoon in the vertical transport of the Nabro plume. In response to this study Fromm et al. (2013) and Vernier et al. (2013) assert that the initial eruptive plume was injected directly into the stratosphere. One piece of evidence comes from brightness temperature imagery of the early plume showing temperatures around the cold point tropopause and evidence of overshooting in the stratosphere. Fromm et al. (2013) also show observations from the Microwave Limb sounder (MLS), including a SO_2 layer at 19 km one day after the eruption and several stratospheric enhancements after that. They also point out the existence of a CALIOP observed aerosol layer at 18.5 km on 16 June which can be traced back to the Nabro eruption. Vernier et al. (2013) present a comprehensive CALIOP analysis. A cumulative plot of aerosol top heights in the Middle East and Asia in the first week after the eruption reveals that a large part of the Nabro plume attained heights between 15 and 19 km, above or near the local tropopause. Bourassa et al. (2013) rebut most of these arguments and provide additional evidence supporting the conclusions of their original study. Their strongest arguments are based on MLS SO_2 measurements in the early plume. Although these exhibit stratospheric SO_2 enhancements, the majority of the SO_2 load in these profiles is found in the troposphere. Further down the transport path on 18 June SO_2 enhancements are found in the stratosphere without coincident tropospheric enhancements, which provides further supporting evidence of uplift.

The analysis of Bourassa et al. (2012, 2013) does provide pieces of evidence for entrainment and uplift of the Nabro plume by the Asian Monsoon. On the other hand, the analyses of Fromm et al. (2013) and Vernier et al. (2013) do seem to indicate that at least part of the initial plume reached the UTLS. To prove or disprove the Asian Monsoon scenario and reconcile the different observations, analysis should quantitatively take into account the relative weight of the different injection heights, and ideally should also focus on observations of the actual uplift. Another important point not addressed by the aforementioned studies is that Nabro injected considerable amounts of high altitude SO_2 for at least 4 days (Theys et al., 2013) after the start of the eruption. Their role on the observed stratospheric loadings needs to be investigated.

For this particular eruption, limb or lidar measurements suffer from a lack of spatial resolution. In addition, no CALIOP data was available for the first two days of the eruption. Recently, the potential of the Infrared Atmospheric Sounding Interferometer (IASI) (Clerbaux et al., 2009) onboard Metop-A to retrieve vertically resolved SO_2 clouds with high precision was demonstrated (Carboni et al., 2012). In this paper, we introduce and validate a new but related retrieval approach and use it to analyse the Nabro eruption. IASI's bi-daily global coverage allows us to study the Nabro plumes at unprecedented spatial, temporal and vertical

resolution. The goal of this paper is threefold: (i) to present a new unconstrained and fast SO_2 height retrieval algorithm, (ii) to validate this new algorithm using CALIOP measurements, (iii) to study the injection height of the Nabro eruption and the role of the Asian Monsoon on the plume transport. In the next section, we detail the new algorithm, discuss how it differs from other algorithms and highlight its relevance for near-real time applications. In Sect. 3, SO_2 retrieved heights are presented for the Nabro eruption plume, accompanied by a comprehensive validation using CALIOP measurements. In the final section we discuss the results in light of the controversy, and present our conclusions.

2 SO_2 height retrievals

Recently a very sensitive trace gas detection method was introduced for high spectral infrared measurements (Walker et al., 2011, 2012). Consider a spectral retrieval of a trace gas total column $\hat{x}$ of the form (we assume that the background target columns x are negligible)

$$\hat{x} = (\mathbf{K}^T \mathbf{S}^{-1} \mathbf{K})^{-1} \mathbf{K}^T \mathbf{S}^{-1} (\mathbf{y} - \bar{\mathbf{y}}), \qquad (1)$$

with $\mathbf{y}$ the observed spectrum, $\bar{\mathbf{y}}$ a background spectrum and $\mathbf{K}$ the derivative with respect to the target species. This is the maximum likelihood solution corresponding to the forward model $\mathbf{y} = \bar{\mathbf{y}} + \mathbf{K}x + \epsilon$ and with Gaussian instrumental noise ϵ characterised by a covariance matrix $\mathbf{S}$ (Rodgers, 2000). Here linearity is assumed as well as exact knowledge of all atmospheric parameters affecting the spectrum in the spectral range under consideration. In reality this knowledge is not available, and other unknown quantities (such as the surface temperature and water vapour for SO_2 retrievals) need to be taken into consideration. However, instead of retrieving these parameters, they can also be considered as permanent unknowns and incorporated in a generalised noise covariance matrix. In the linear case, such a solution is equivalent to the one obtained by simultaneously retrieving all interfering unknowns (von Clarmann et al., 2001; Rodgers, 2000). For species which are rarely observed in IASI spectra, constructing such a generalised noise covariance and associated background spectrum is easy, as it can be simply constructed from a random sample of spectra uncontaminated by the target species. This is the essence of the Walker et al. (2011, 2012) method. Despite its relative simplicity, test cases have revealed that it is about an order of magnitude more sensitive than previously used detection methods. The conditions of the retrieval, namely constant Jacobians $\mathbf{K}$ and linearity are usually not satisfied. The quantity $\hat{x}$ is therefore an apparent column which should be interpreted as a qualitative estimate of the column. For these reasons it is convenient to normalise this apparent column as

$$Z = \frac{\mathbf{K}^T \mathbf{S}^{-1} (\mathbf{y} - \bar{\mathbf{y}})}{\sqrt{\mathbf{K}^T \mathbf{S}^{-1} \mathbf{K}}}. \qquad (2)$$
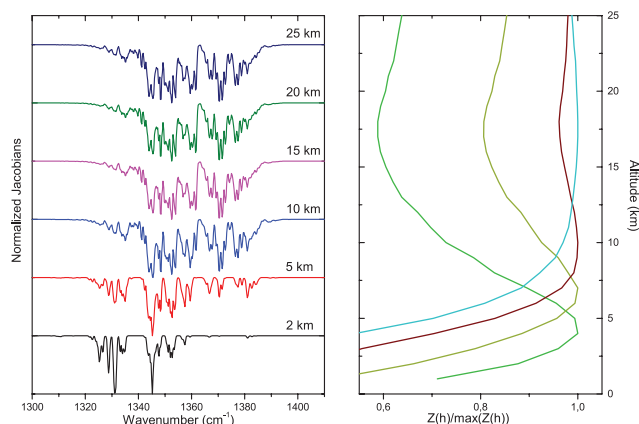
This Z number is unitless and has a mean of zero and a standard deviation of one on uncontaminated spectra (Walker et al., 2011; Clarisse et al., 2013). It represents the number of standard deviations away from the average and the larger its value, the more likely it corresponds to an enhancement of the target species (Walker et al., 2012).

The real strength of the detection method stems from being able to use a large spectral range and a covariance matrix which characterises IASI measurements better than any traditional forward model could do. The SO_2 retrieval method presented in Carboni et al. (2012) uses a related approach to retrieve SO_2 columns and plume heights. It differs from the detection method in three ways. First, the covariance matrix is built from spectral residuals between observed spectra and spectra simulated by a forward model fed with the best possible knowledge of the local temperature and humidity profiles. Secondly, the maximum likelihood retrieval is replaced by an iterative Levenberg–Marquard retrieval with variable Jacobians. Here the SO_2 column is assumed to be confined to a narrow altitude band and the Jacobians are then calculated with respect to the column and the height of this band. The third difference is the use of a priori information and a covariance matrix which constrains the retrieval. Retrievals performed in this way, then yield quantitative estimates of the column amounts and heights, as opposed to the apparent columns discussed above. The use of a generalised covariance matrix still preserves some of the advantages of the detection method, in particular enhanced sensitivity and being able to fully take into account the limitations of the forward model.

Here we propose a hybrid method to retrieve SO_2 plume heights. Let us define a Z function

$$Z(h) = \frac{\mathbf{K}_h^T \mathbf{S}^{-1} (\mathbf{y} - \bar{\mathbf{y}})}{\sqrt{\mathbf{K}_h^T \mathbf{S}^{-1} \mathbf{K}_h}}, \qquad (3)$$

with $\mathbf{K}_h$ the Jacobian with respect to the SO_2 partial column at an altitude h. When an observed spectrum contains a detectable amount of SO_2, this Z function should attain values significantly larger than 1. The Jacobians $\mathbf{K}_h$ contain the SO_2 signature that can be expected at an altitude h, and the Z function should therefore peak at h. Another way of seeing this is that Eq. (3) is a covariance weighted normalised projection (Clarisse et al., 2013) of the observed spectrum onto a SO_2 signature relevant to the different heights. When Z reaches its maximum there is maximal overlap between the observed spectrum and the SO_2 signature at that altitude. Simply calculating $Z(h)$ for different altitudes h and finding the maximum thus gives a viable and fast way of estimating SO_2 plume altitude. Example Jacobians in the range 1300–1410 cm^{-1} and $Z(h)$ for different observed spectra are presented in Fig. 1. For this example, large differences in the Jacobians can be observed up to an altitude of 15 km. This is logical as most of the altitude information comes from interference of the SO_2 absorption lines with the water vapour
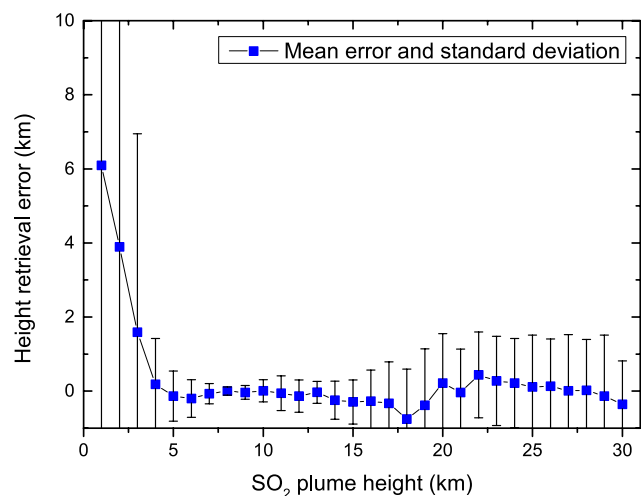
Fig. 1. (Left) Jacobians with respect to a SO_2 layer at different altitudes. They have been normalised and offset for display purposes. (Right) The Z function acting on different observed IASI spectra of Nabro. The values have been normalised to ease comparison.

Fig. 2. Theoretical height retrieval error biases and standard deviations constructed from a simulation of 10 000 IASI spectra with SO_2 altitudes between 1 and 30 km.

band. This is reflected in the $Z(h)$ profiles shown on the right. At low altitudes, these peak sharply, and become broader as the altitude increases.

To test the theoretical accuracy of this method for different altitudes, 10 000 forward simulations of 5 DU SO_2 clouds between 1 and 30 km were carried out. To make the simulation as realistic as possible, spectral noise was added to these spectra. This noise was generated from the multivariate normal distribution with the mean bias and covariance matrix used for the quantitative SO_2 column retrievals (see end of this section). Calculating spectra in this way is a realistic way of simulating real observed spectra because biases in the forward model are removed, and because instrumental noise is added. However, note that the atmospheric parameters used in the simulation are the same as the ones which were used to construct the Jacobians. Using this method we hence obtain upper bounds on the accuracy of the algorithm.

The results are summarised in Fig. 2. As expected from the $Z(h)$ profiles shown in Fig. 1, the best accuracy is achieved between 5 and 15 km with error bars below 500 m. Below 3 km the tropical atmosphere is almost opaque in the spectral range of interest due to water vapour, and the algorithm therefore loses its accuracy drastically (a dryer atmosphere would allow to penetrate lower down). Above 18 km, the error bar is almost constant at around 1.5 km. At these altitudes, the water vapour content in the atmosphere is low, and the fact that such a good sensitivity is achieved is related to pressure and temperature dependence of the SO_2 lines (Clerbaux et al., 2008). Although hard to see with the naked eye on apodized IASI spectrum, the simulation demonstrates that altitude information is contained in the spectrum even in the stratosphere.

Another appealing aspect of the algorithm is the performance on scenes with overlaying meteorological clouds. Cloudy scenes are at no stage in the algorithm treated

separately. Hence, it could be argued that as water in the gas and in the liquid phase have a similar broad band extinction across the infrared spectral region that these will have an important effect. However, as we will show later, clouds seem to have little effect on the retrieved altitudes of this hybrid method, as long as they are not completely masking the SO_2 layer below. The reason is that while the broad extinction of clouds and water vapour is present in the Jacobians, these also exhibit the sharp spectral lines of water vapour in the gas phase, which are not found in clouds.

This hybrid method has the benefit of relying on the forward model just for its Jacobians. These can be precalculated once and the remaining calculations then become trivial. In other words, this method is suitable for near real time applications and can be implemented in operational centres with minimal computational resources. It would for instance be a good candidate for implementation in the SACS project (Brenot et al., 2013), dedicated to timely warning of volcanic plumes. Another benefit is that the algorithm uses no a-priori information or constraints on its retrieval. Especially for smaller loadings, there is always the possibility of a constrained height retrieval algorithm to get stuck in a local minimum near its a priori. It also has some disadvantages, the main one is probably its performance for heavily saturated plumes. In this case, the Jacobians that are calculated in the neighbourhood of small loadings are no longer representative. Fortunately, saturation occurs only in very young plumes, and even in these cases, altitudes can be estimated from the plume edges, away from saturation.

In what follows, we have interpolated pixels with a Z value larger than 250 or an altitude larger than 23 km from nearby pixels. The latter condition was found to be good at removing isolated rogue detections just above or below IASI's detection limit. Jacobians were calculated with Atmosphit

(Coheur et al., 2005) using average atmospheric conditions representative for $10° \times 20°$ latitude/longitude boxes in the Northern Hemisphere in June 2011. Average water vapour and temperature profiles were calculated in each box from the Eumetsat IASI L2 data of several days in June 2011. In each case, Jacobians were generated representative for plumes between 1 and 30 km in steps of 1 km, with a 1 km thick layer of 5 DU of SO_2. For each specific observation, local Jacobians were then obtained using a bilinear interpolation of the four closest grid boxes. For operational applications Jacobians would need to be precalculated for such boxes and different time-periods of the year. For the construction of the global mean spectrum $\bar{y}$ and the global error covariance matrix $\mathbf{S}$ we used one million random IASI spectra selected from all periods of the year from around the globe. Spectra with observable SO_2 features were filtered out recursively (analogously as was done in Clarisse et al., 2013).
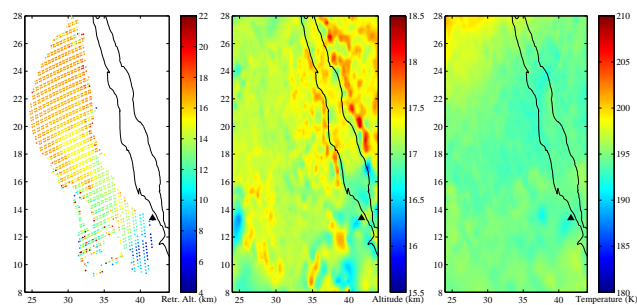
Below we also calculated column retrievals for selected days. These were obtained using an iterative optimal estimation fit, very similar to the one presented in Carboni et al. (2012) as explained above. Atmospheric water and temperature profiles were taken from the collocated Eumetsat IASI L2 data. As we retrieve altitude independently, the fit is one-dimensional with only the magnitude of the SO_2 column that needs adjusting. For this retrieval a different mean spectrum and covariance matrix are needed, ones that are built up from spectral residuals (see above). Here we used 15 000 forward simulations, over randomly chosen locations and times of the year. Again no distinction is made between cloudy and cloud-free scenes as the algorithm is largely robust for the presence of clouds (Carboni et al., 2012).

3 Results for Nabro

3.1 The first day

The first IASI observations of the plume were made on the morning of 13 June. Unfortunately, close to the equator there is an observational gap between different orbits which covers a large part of the plume. Therefore, and also because of saturation issues, we focus on the evening orbit of the 13th. SO_2 height retrievals are shown in Fig. 3. Displayed altitudes reach from 4 km close to the volcano to 17 km furthest downwind.

Central to the discussion on the Nabro injection height is the question whether it is situated above or below the tropopause. Quite a bit of the disagreement regarding Nabro stems from the use of different definitions of a stratospheric plume. Some in terms of altitude, some in pressure, some in terms of potential temperatures and some as a combination of these. It is difficult to assign fixed thresholds on any of these, as the tropopause is highly variable with latitude. Answering the question on a stratospheric injection from transported plumes is therefore very complicated, and in our opinion only

Fig. 3. (Left) IASI retrieved SO_2 altitudes on 13 June (evening overpass). (Middle) Altitude of the tropopause on 14 June (derived from Eumetsat IASI L2 data). (Right) Temperature at the tropopause on 14 June (derived from Eumetsat IASI L2 data).
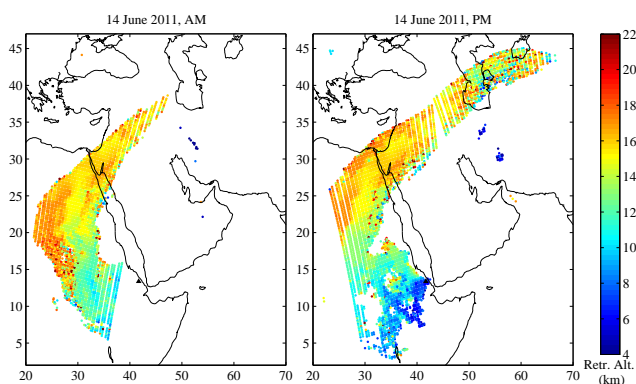
data from the young plume should be used to study the injection height.

Here we adopt as definition of the tropopause, the first altitude level above 4 km which has a lapse rate below $0.1\,\mathrm{K\,km^{-1}}$. In the tropics this corresponds to the cold point tropopause, while for higher latitudes it is close to the definition adopted by the World Meteorological Society (see also Birner, 2010). Figure 3 depicts the IASI level 2 (IASI L2) derived tropopause altitudes and temperatures for the 14th (the data on the 13th gave unreasonable low altitudes coincident the volcanic plume, pointing to a problem with the level 2 data due to the effect of the plume on the retrieval algorithm). In the relevant region the tropopause is at 17 ± 0.5 km and 195 ± 3 K. This altitude range matches our plume height maximum. The brightness temperature imagery shown in Fromm et al. (2013) and Vernier et al. (2013) indicate a temperature around 195 K also for a large part of the plume. Finally SO_2 MLS data shown in Bourassa et al. (2013) also show the largest enhancements of SO_2 around 17 km. These pieces of information together strongly indicate that the early Nabro plume was injected mostly at altitudes between 15 and 17 km with at least part near the thermal tropopause at 17 km. The tropopause acts as a natural barrier for vertical transport, so it is not surprising to find our measured maximums at this altitude. Note that the radiosonde temperature profile shown in Bourassa et al. (2013) has the tropopause at 18.1 km, but was located on the other side of the Red Sea, where the IASI L2 also indicates a slightly higher altitude. The imagery shown in Fromm et al. (2013); Vernier et al. (2013) reveals a small part of the plume being overshot in the stratosphere. The presented IASI retrievals did not capture this, possibly because of our specific treatment of saturated levels. IASI mass retrievals for this day indicate a mass not larger than 400 kT for plumes above 10 km.
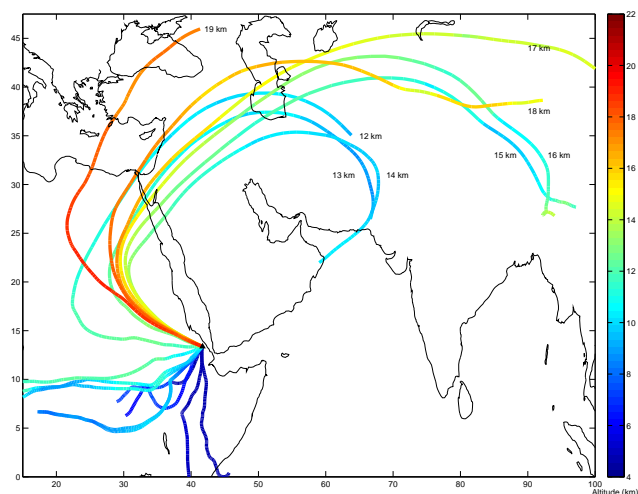
3.2 The second day

Altitude retrievals for the 14th are shown in Fig. 4 for the morning and evening overpass. Four different parts can be

Fig. 4. IASI SO$_2$ altitude retrievals for 14 June for the morning (left) and evening (right) overpass.
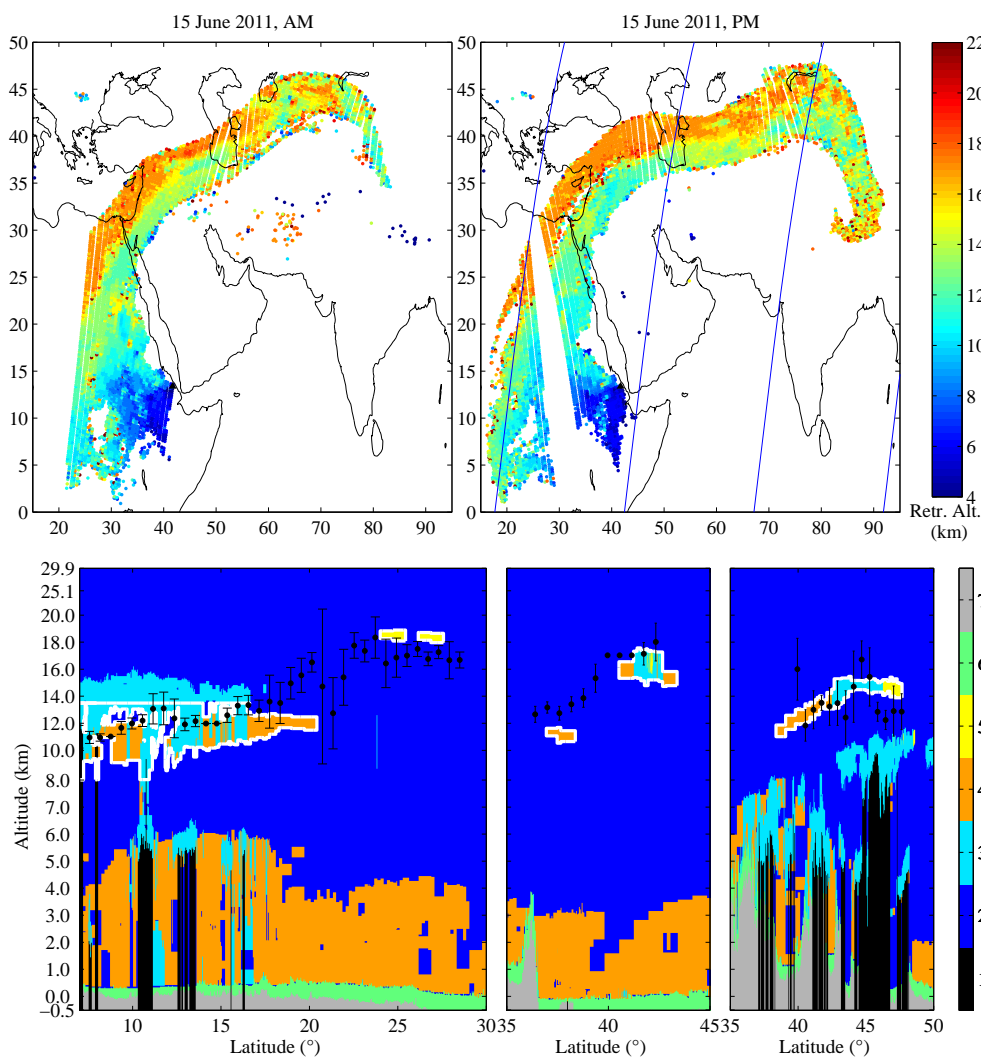

Fig. 5. HYSPLIT trajectories of an instantaneous injection from Nabro at 22:00 UTC on 12 June 2011 with injection heights ranging from 3–19 km for a period of 5 days. The colours of the trajectories indicate the forecasted altitude, rather than the injected altitude.

distinguished: (i) a part below 13 km south of 20° latitude (ii) a higher altitude part at 17–18 km and mostly on the western (AM) and northwestern (PM) side of the plume (iii) the middle part of the plume around 15–16 km and finally (iv) the part furthest downwind of the plume at altitudes 13–14 km (PM only). For 14 June, brightness temperature imagery cannot be used as these are only indicative for altitudes for opaque plumes. Also for that day, there are no CALIOP measurements available. We therefore resort to forward trajectory modelling to compare the altitude retrievals with, even though caution has to be exercised in drawing conclusion from such data alone. An analysis using ECMWF data and Flexpart revealed for instance the difficulty in simulating transport for the first 15 h of the eruption (Theys et al., 2013). On top of that, using different windfield datasets can yield differences in the simulated trajectories. Here we simulated forward runs using the GDAS dataset with HYSPLIT (Draxler and Rolph, 2013) as shown in Fig. 5. These trajectories are compatible with transport towards East Asia for altitudes in the range 12–18 km, towards the west/southwest with altitudes 5–11 km and towards the south at even lower altitudes. These overall patterns are well captured in the IASI SO$_2$ height retrievals. In addition, a closer look at the different parts of the observed plume and changing altitude of the forward trajectory (changing colour along transport in Fig. 5) reveals that the trajectories match the retrieved SO$_2$ transport features. This is straightforward to see for the low (i) and the high (ii) part. Note that the latter reaches altitude up to 18 km in the AM overpass (for the PM this part of the plume is cut off by the satellite orbit). This small part of the plume coincides with an observed CALIOP feature around 18.5 km on 15/16 June as shown in Bourassa et al. (2012) and recognised as such in Fromm et al. (2013) (see also Fig. 6). This confirms that there was overshooting in the stratosphere of a part of the plume. Part (iii) and (iv) between 13 and 16 km correspond well with the transported trajectories at 16 and 17 km. These plume segments, presumably originating at 16–17 km according to the IASI 13 PM retrieval, therefore seem

to descent considerably in the course of 48 h. For these, the IASI height retrievals are again fully consistent in space and time with the HYSPLIT trajectories. IASI mass retrievals for this day indicate a mass not larger than 600 kT for plumes above 10 km, and about 200 kT below.

3.3 The first week

IASI plume height retrievals and coincident CALIOP measurements for 15–19 June 2011 are presented in Figs. 5–9. We first discuss and interpret the IASI retrievals, for which the following observations can be made:

- Nabro released SO$_2$ almost without interruption in the first week, but with large variations in magnitude and altitude. Plumes emitted below 10 km travelled consistently south/southwest at a moderate speed. These plumes could be followed up to maximum a week, but not longer, consistent with the short lifetime of SO$_2$ at low altitude. The total emitted SO$_2$ mass for plumes below 10 km is considerable, a selected mass retrieval for the 15th alone gives a lower bound of around 800 kT.

- The transport patterns observed in the first two days are confirmed by the observations on the 15th: plumes above 10 km travelled first north toward the Mediterranean Sea, and then east over the Caspian Sea along the prevailing subtropical jet stream and the rest of the large Asian monsoon anticyclone. Vertical wind shear pushed the higher parts above 15 km further north than the lower parts which travelled somewhat faster downwind. This circulation within the monsoon is valid for the initial eruption plume from the 13th, but also for

Fig. 6. IASI SO$_2$ height retrievals are presented on top from 4 to 22 km; blue lines indicate CALIPSO ground tracks within 5 h of the plume. In the bottom panels, the CALIOP the Level 2 product, "Vertical Feature Mask" is shown for the CALIPSO curtains corresponding to the ground tracks shown above, from left to right. Colours are numbered 1 to 7 indicated in the colour bar and stand for: no signal (1), clean air (2), cloud (3), aerosol (4), stratospheric feature (5), surface (6) and subsurface (7). Features which are likely to correspond to sulfate aerosols originating from Nabro are contoured in white on the CALIOP maps. Coincident IASI altitude retrievals are superimposed on these CALIOP maps as black dots, with a standard deviation representing the spread in retrieved altitudes around the overpass.

the rest of the volcanic emissions in the first week. For the 15th the total SO$_2$ mass adds up to around 650 kT for the plumes above 10 km.

– The parts of the plumes which reached Eastern Asia are mostly confined within the Asian monsoon anticyclone, sending the plume back westwards. These resulting western moving plumes are predominantly situated around the tropopause at 17 km. This is just above the top of the highest clouds observed in coincident CALIOP measurements (best seen on 17–19 June). The sequence of height retrievals from the 15th to the 18th, provides evidence for rapid uplift of the mid-tropospheric plumes at 12–15 km up to

the tropopause (even though partial washout of these plumes cannot be excluded). This seems valid for the parts that underwent descent after being initially injected at the tropopause, but also for those parts that were injected at lower altitude. No such rapid uplift is observed for those filaments already at the tropopause before entering Eastern Asia. It is not possible to estimate the total amount of sulfur that eventually ended up around the tropopause using IASI measurements alone, given the nature of this dynamic Nabro plume with continuous new injections of SO$_2$ and variable removal processes in moving airmasses.
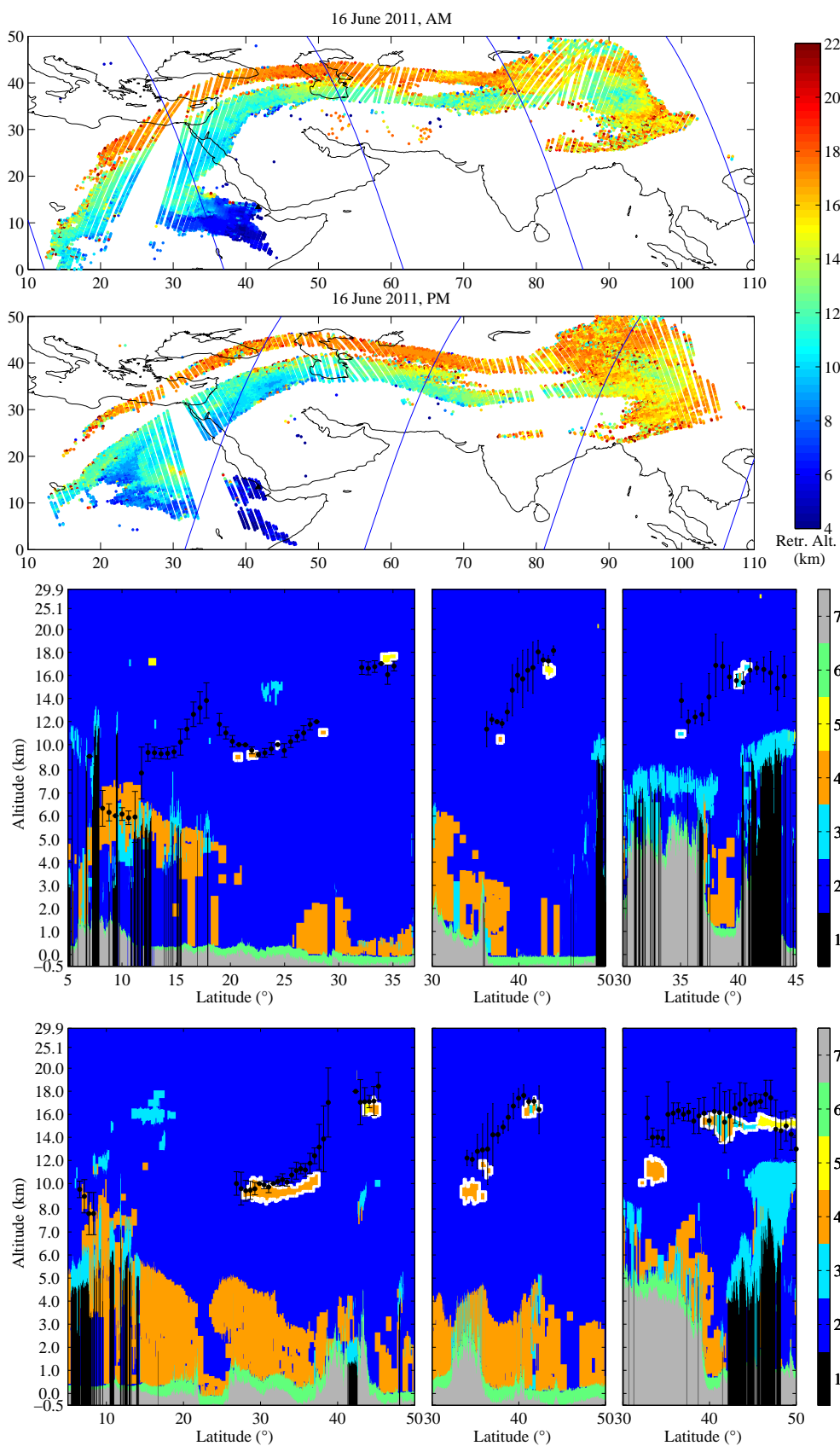
Fig. 7. Same as Fig. 6 for 16 June 2011.

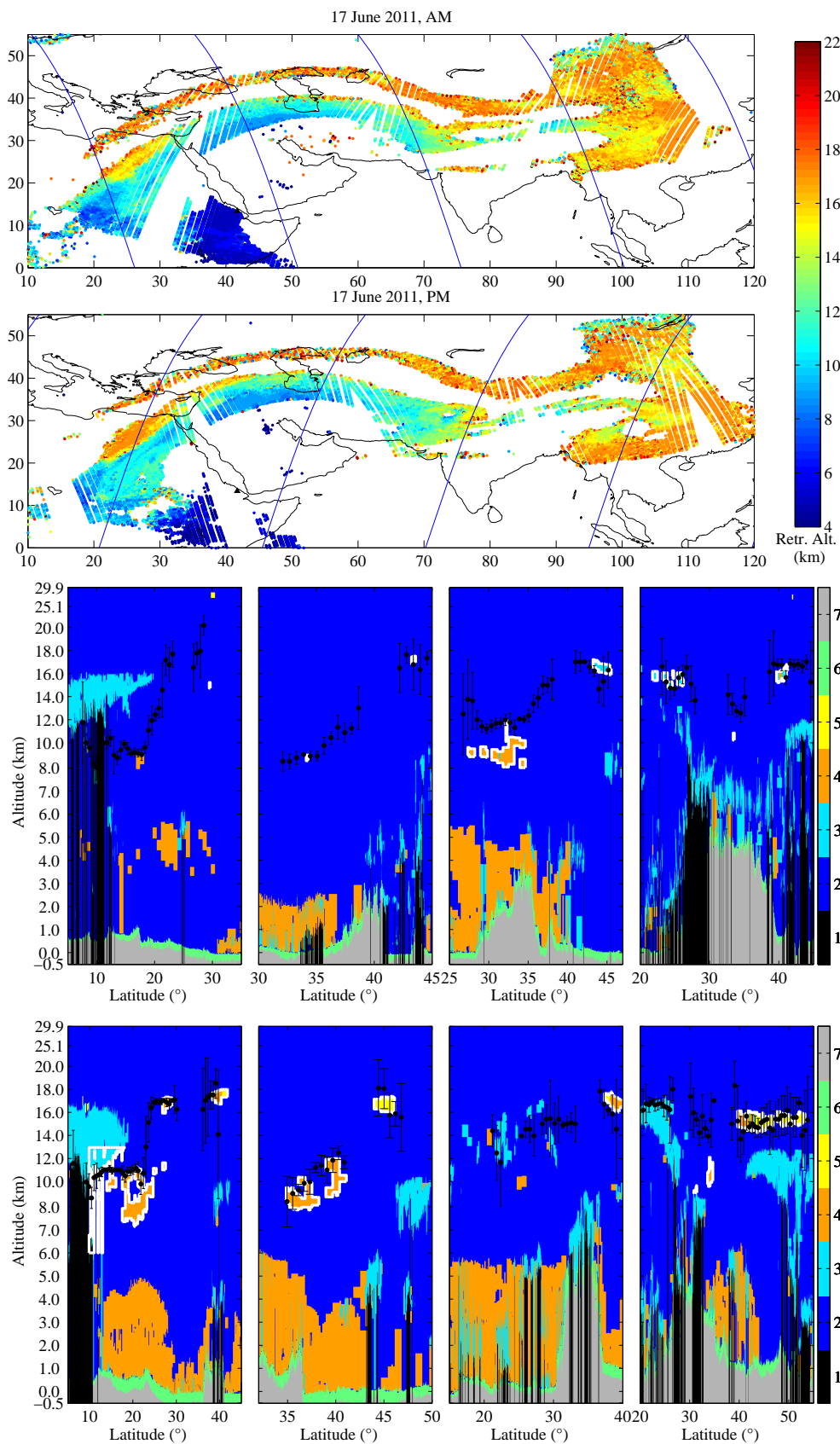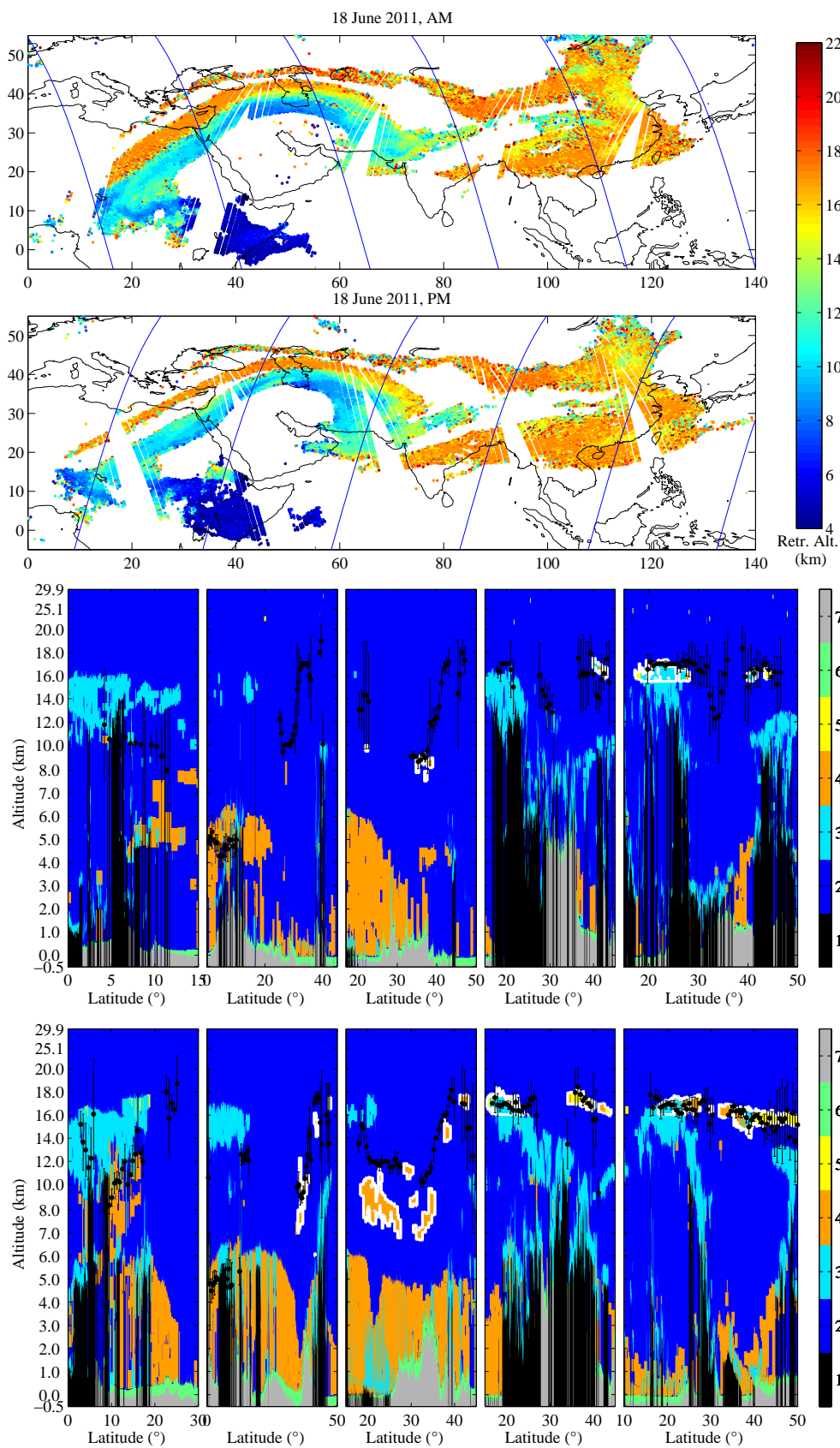**Fig. 8.** Same as Fig. 6 for 17 June 2011.

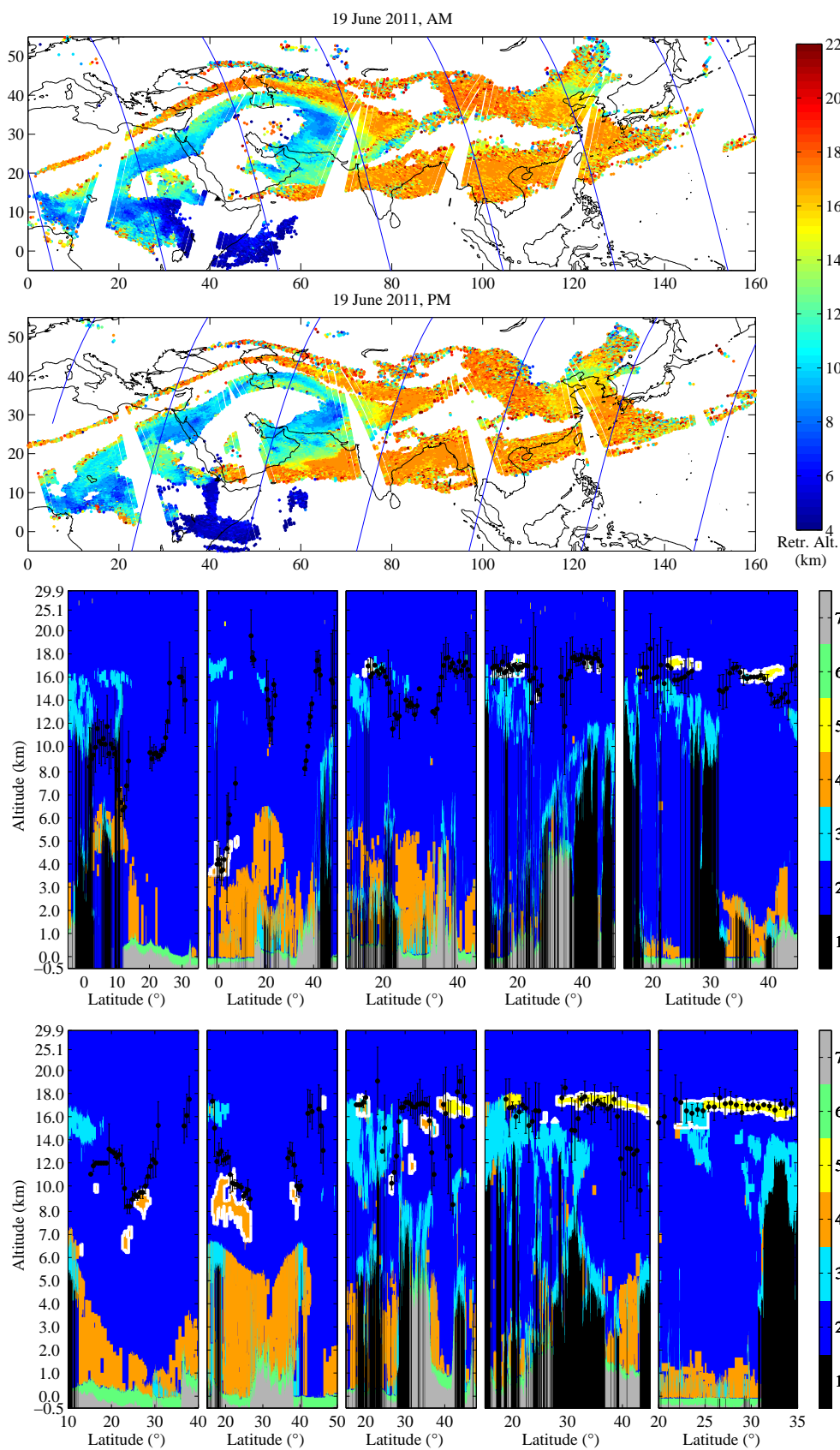**Fig. 9.** Same as Fig. 6 for 18 June 2011.

Fig. 10. Same as Fig. 6 for 19 June 2011.

- Part of the plume over Eastern Asia is transported first to the north, but later these filaments do turn to the east and over the Western Pacific. From here, one part is entrained in the anticyclone, whilst the other part travels further over the Pacific. This moderate leaking out of the Asian Monsoon circulation is a constant pattern observed for all observations after the 19 of June (not shown here). There is also a complementary but weaker transport out from the west side of the Anticyclone over Central Africa. These two transport pathways are the two main escape routes from the anticyclone circulation, and while they are slow, they seem responsible for the spreading of the Nabro plume over the whole Northern Hemisphere (Bourassa et al., 2012).

- From the 17th onwards, the smaller Iranian anticyclone centred over the Zagros Mountains and the Persian Gulf (Zarrin et al., 2011) entrains most of the Nabro plume around 10–13 km, preventing it from being transported further eastwards. No uplift of this part of the plume is observed.

- On the 17th, AM overpass, a marked segment on the western side of the 10–14 km altitude plume over Africa attains altitudes between 15–17 km. In subsequent overpasses this segment covers the whole northern edge of that plume. These observed altitudes are confirmed with coincident CALIPSO overpasses (see below) and are also compatible with its subsequent transport trajectory which tears away from the lower altitude plume on the 18th. Uplift on this side of the monsoon anticyclone seems unlikely, so that this part of the plume was likely emitted at such high altitudes. It can probably be traced back to the small part of the plume around 15–16 km detected on the 16th PM over Sudan (not covered completely by the IASI overpass, and also possibly masked by SO_2 signals from overlapping plume below). On the 19th this filament mixes with the rest of the Nabro plume located at the tropopause over Eastern Asia, further contributing to the total amount of sulfur which reached such altitudes.
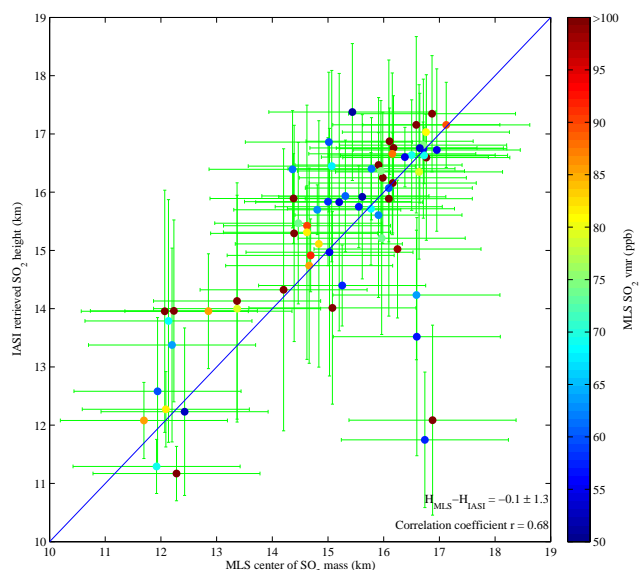
Looking at the different IASI images of retrieved altitudes and the trajectory analysis presented before, it is apparent that the presented product is particularly self consistent, i.e. homogeneous in time and space, and almost unaffected by other atmospheric parameters (water vapour, clouds) or topography. The IASI height retrievals seem almost unaffected by the strength of the SO_2 signal as long as it is detectable with confidence (Z value above 5). This can best be seen from the plume edges which are on the same altitude level as neighbouring pixels towards the centre of the plume. It is also evident from the retrievals on the 19th, which shows an aged plume with most columns below the 1–5 DU level. This

is unexpected as a larger signal naturally increases the signal-to-noise ratio and information content. SO_2 height retrievals from the OMI instrument for instance become only reliable for columns above 20–30 DU (Yang et al., 2010; Nowlan et al., 2011).

For an absolute comparison, we present in Figs. 5–9 coincident CALIOP measurements underneath the IASI retrievals. While these instruments measure different things, sulfate aerosol is expected to travel alongside SO_2 as it is oxidized from it. Here we chose to plot the CALIOP vertical feature mask product, which is a level 2 product (Winker et al., 2009) that identifies and classifies observed features. It is useful to distinguish clouds from other aerosols, and makes it easier to identify volcanic plumes than from the level 1 data. Careful manual analysis of the level 1 does however point to occasional misclassification. In addition, the feature masks sometimes misses thinner filaments which could be identified from the level 1 (especially in hindsight, when comparing with the IASI product). For illustration purposes, white contours have be drawn around features which likely correspond to the Nabro plume. In case of doubt, this was done with the aid of an analysis of the depolarization ratios, which are expected to be very low for sulfate aerosols (Vernier et al., 2013). For the comparison, IASI retrieved mean and standard deviations of the altitudes in a 0.5° radius along the CALIPSO overpass have been used. One should however be wary that the observations are never totally coincident because of the timelapse in the overpass of the two instruments (IASI first, then CALIOP about 3 h later), which can cause a large difference in the observed altitude.

Despite these limitations, altitude discrepancies between observed IASI retrieved SO_2 altitude and CALIOP aerosol measurements are for the most part, less than 2 km. It is remarkably good for plumes in the range 16–18 km, which are more often than not captured within a 1 km error bar. The largest discrepancies seems to be for plumes around 8–9 km, which are in about half of the cases put at altitudes around 10–11 km. But even for these, it is striking how well the gradient within the plumes are captured (for instance on the 18 June 3rd PM overpass). Almost no coincident plumes below 7 km were found in the analysis of CALIOP data, because of the limited coverage of CALIOP coupled with the smaller sizes of the plumes. And even in those cases where there was a good overpass, interference of other lower tropospheric aerosol (e.g. desert dust) made identification of volcanic aerosol impossible in the CALIOP data. As mentioned before however, the plumes at lower altitude are almost certainly identified correctly based on their transport pathway and shorter lifetime. The CALIOP data reveals that the performance of the algorithm for plumes located below meteorological clouds, is not any worse than in cloud free scenes.

Another independent validation of the IASI measurements can be obtained from coincident MLS measurements of SO_2. A scatter plot of IASI height retrievals vs. the centre of mass height from MLS is shown in Fig. 11 for 13–20 June. Here

Fig. 11. Comparison of MLS centre of SO_2 mass with coincident IASI SO_2 height retrievals in a 200 km radius around the MLS measurements. The MLS errorbar was taken fixed at ± 1.5 km, the IASI errorbar depicts the standard deviation of the coincident IASI measurements. MLS data is from the v3.3 EOS MLS Level2 which was downloaded from the NASA Goddard Space Flight Center, Data and Information Services Center (http://disc.gsfc.nasa.gov/).

both retrievals were separated in the day and night overpass and all IASI measurements within a 200 km radius of the MLS measurement where used. Only measurements with a volume mixing ratio above 50 ppb were used for MLS. Given the measurement uncertainties of both products, the plot reveals a good match between both instruments, with a mean bias of -0.1 km, a standard deviation of 1.3 km and a correlation coefficient of 0.68.

3.4 The aging plume

The transport of the high altitude Nabro plume follows the Asian monsoon anticyclone for many weeks, with the majority of the plume invariably located between 16 and 18 km, both from IASI and CALIOP. An example is shown in Fig. 12 for 30 June 2011. The agreement between the two instruments is not as good as it is during the early days of the plume, especially in the parts where the aged higher altitude plume overlays fresher lower altitude plumes. Here the IASI algorithm often (and naturally) retrieves the lower plume, as this one has the larger concentrations of SO_2; whereas CALIOP is more sensitive to the aerosols in the aged plume. Overall this figure provides strong evidence that the Nabro plume was located around the tropical tropopause for at least two weeks after the initial eruption.

Around 30 June, SO_2 maximums are around the 1 DU level, and altitude retrievals gradually becomes more difficult and noisy. To get a better view on longer term plume

movement, a time series of the relative frequency of detected IASI SO_2 altitude is shown in Fig. 13 for 14 June to 15 July. The most striking feature in this plot is the apparent gradual uplift of the plume mostly situated at 17 km to altitudes of 18–19 km. Two CALIPSO overpasses on the 10 and 15 July over the Middle East, which is the region where SO_2 is detected for the longest period of time, are shown in Fig. 14. These confirm that compared to 30 June the plume has risen slightly, with a mean altitude around 18 km (and a spread mostly within 17–19 km) for the 15th. This gradual uplift above the tropopause is fully consistent with the uplift observed by OSIRIS (Fig. 2 in Bourassa et al., 2012). The coincident IASI retrievals are also shown on Fig. 14. Instead of the mean, we show for these aged plumes the mode (the most frequent retrieved altitude) within a 0.5° radius of the CALIPSO overpass. This mode is more representative of the large scale aged plume and less affected by noise, whereas the mean underestimates the prevalent altitude due to the presence of anomalous low altitude retrievals. Even for these month-old plumes with sub-dobson level SO_2 columns, the altitudes retrieved in this way are within the ± 2 km uncertainty.

4 Conclusions

In this paper we have presented a new algorithm for IASI SO_2 plume altitude retrievals. Trajectory analysis and coincident CALIOP and MLS measurements reveal an agreement predominantly within 2 km for plumes up to the 1 DU level. Given IASI's global bi-daily coverage and the attractive computational properties of the algorithm, this opens perspectives for a large number of applications including near real time uses (e.g. hazard mitigation) and for off-line analysis (e.g. study of 3-D circulation patterns).

With respect to the Nabro eruption, we have presented evidence that the initial plume was injected at altitudes between 15 and 17 km. A smaller part was injected higher up reaching 18.5 km according to CALIOP measurements. Within the Asian Monsoon anticyclone, this initial plume was seen to undergo a partial descent on the western side of the anticyclone. Eventually the initial plume ascended to thermal tropopause around 16–18 km over Eastern Asia. Apart from the initial eruption, the continuous and large emissions of SO_2 above 10 km up until at least 16 June also likely contributed to the total stratospheric sulfur injection (including a smaller plume in the upper troposphere on the 16th). These emissions were entrained either by the Asian monsoon or the Iranian anticyclone. In the first case they joined the initial injection plume through ascent on the eastern side of the Asian monsoon. The Iranian anticyclone became important after the 16th, and parts of the plume caught up in it did not reach higher altitudes.

Ascent to the level of the thermal tropopause was of the order of 1 km per day over Eastern Asia. In this paper, we did
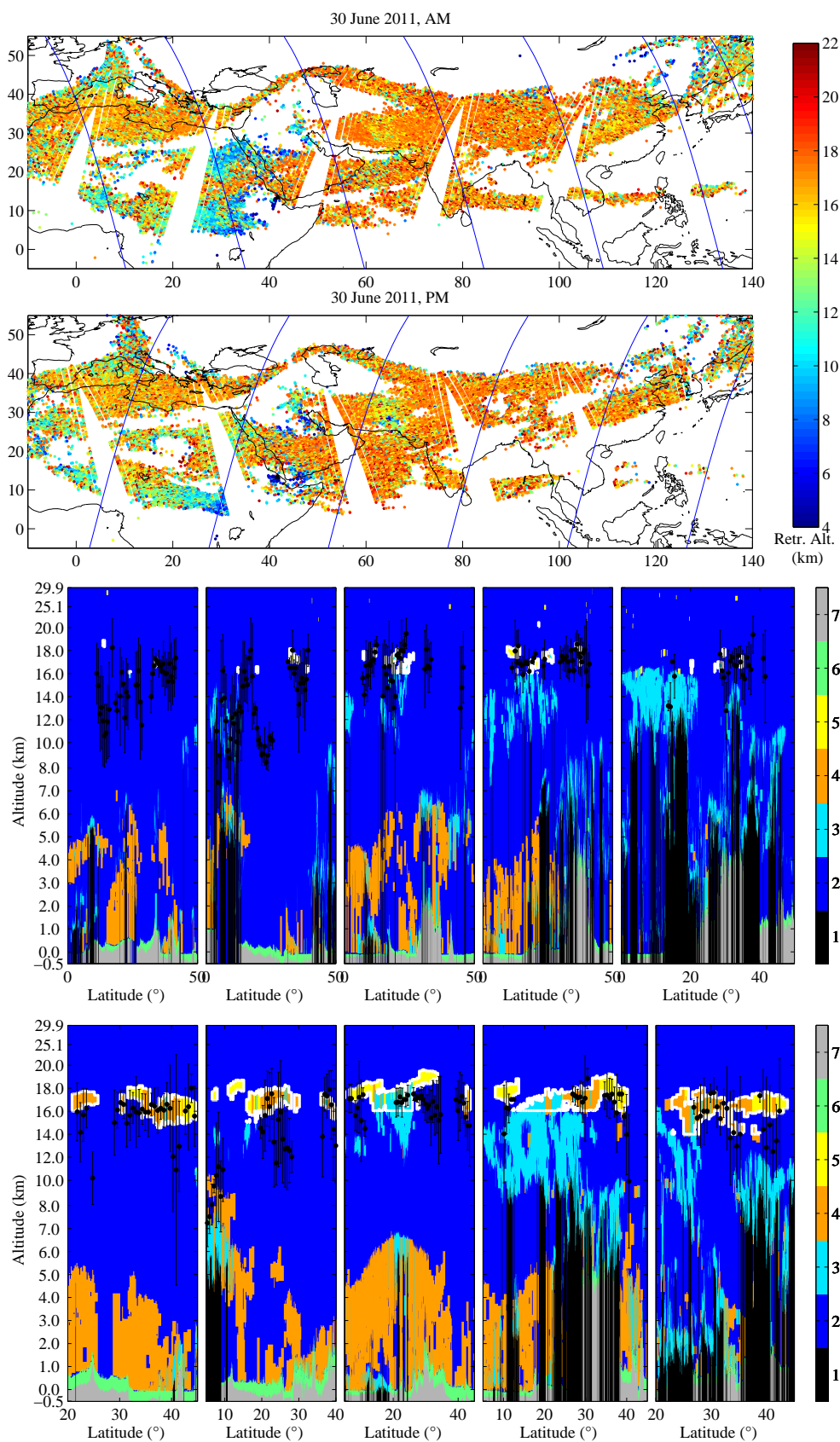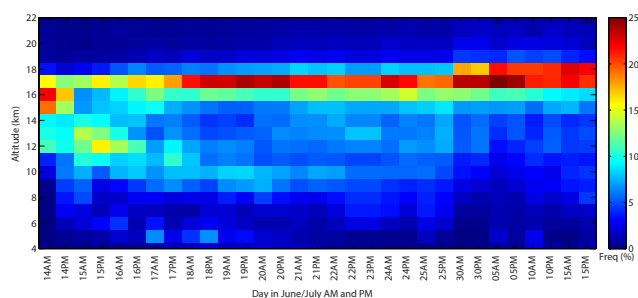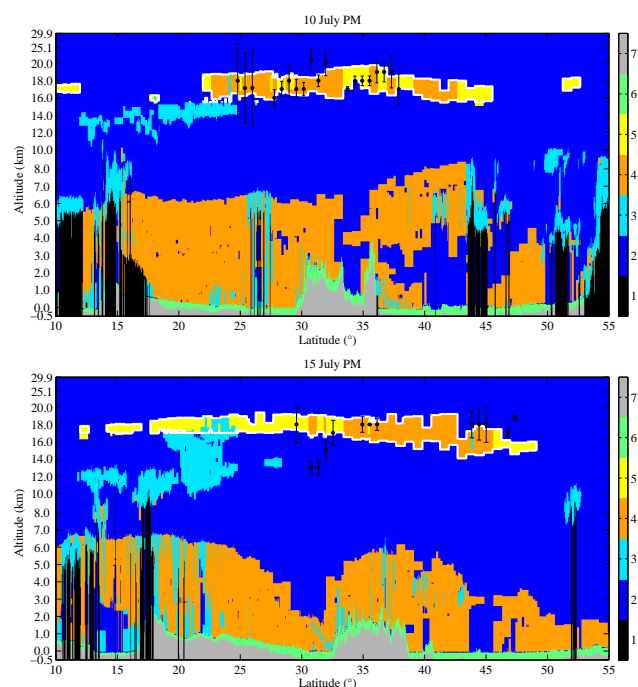
Fig. 12. Same as Fig. 6 for 30 June 2011.

Fig. 13. Frequency of the IASI retrieved SO$_2$ plume height altitude as a function of time for 14 June to 15 July 2011.

Fig. 14. CALIOP measurements for 10 and 15 July (evening overpass) over the Middle East and coincident IASI retrievals (see text).

not address the exact mechanism of the observed rapid descent/ascent of the plume. A recent study suggests that quasi-isentropic flow is enough to explain most of the transport of the Nabro plume (Fairlie et al., 2013). The IASI-observed vertical transport is consistent with isentropic levels sloping downwards towards higher latitude (see e.g. Fig. 3 in Uchino et al., 2012), but a more quantitative approach would be needed to determine whether it explains it completely.

Observed transport into the lower stratosphere was much slower. The vertical resolution of the IASI instrument coupled with the relative short lifetime of SO$_2$ prevents us from presenting conclusions on the location or mechanism of this stratospheric transport, but based on our presented timeseries and OSIRIS averaged profiles (Bourassa et al., 2012) we estimate this ascent to be of the order of 1 km in two weeks.

References

Bergman, J. W., Jensen, E. J., Pfister, L., and Yang, Q.: Seasonal differences of vertical-transport efficiency in the tropical tropopause layer: On the interplay between tropical deep convection, large-scale vertical ascent, and horizontal circulations, J. Geophys. Res.-Atmos., 117, D05302, doi:10.1029/2011JD016992, 2012.

Birner, T.: Residual circulation and tropopause structure, J. Atmos. Sci., 67, 2582–2600, doi:10.1175/2010JAS3287.1, 2010.

Bojanowski, A.: Volcano mix-up, Nature Geoscience, 4, p. 495, doi:10.1038/ngeo1222, 2011.

Bourassa, A., Robock, A., Randel, W., Deshler, T., Rieger, L., Lloyd, N., Llewellyn, E. J., and Degenstein, D.: Large Volcanic Aerosol Load in the Stratosphere Linked to Asian Monsoon Transport, Science, 337, 78–81, doi:10.1126/science.1219371, 2012.

Bourassa, A., Robock, A., Randel, W., Deshler, T., Rieger, L., Lloyd, N., Llewellyn, E. J., and Degenstein, D.: Response to Comments on "Large Volcanic Aerosol Load in the Stratosphere Linked to Asian Monsoon Transport", Science, 339, p. 647, doi:10.1126/science.1227961, 2013.

Brenot, H., Theys, N., Clarisse, L., van Geffen, J., van Gent, J., Van Roozendael, M., van der A, R., Hurtmans, D., Coheur, P.-F., Clerbaux, C., Valks, P., Hedelt, P., Prata, F., Rasson, O., Sievers, K., and Zehner, C.: Support to Aviation Control Service (SACS): an online service for near real-time satellite monitoring of volcanic plumes, Nat. Hazards Earth Syst. Sci. Discuss., 1, 5935–6000, doi:10.5194/nhessd-1-5935-2013, 2013.

Carboni, E., Grainger, R., Walker, J., Dudhia, A., and Siddans, R.: A new scheme for sulphur dioxide retrieval from IASI measurements: application to the Eyjafjallajökull eruption of April and May 2010, Atmos. Chem. Phys., 12, 11417–11434, doi:10.5194/acp-12-11417-2012, 2012.

Clarisse, L., Hurtmans, D., Clerbaux, C., Hadji-Lazaro, J., Ngadi, Y., and Coheur, P.-F.: Retrieval of sulphur dioxide from the infrared atmospheric sounding interferometer (IASI), Atmos. Meas. Tech., 5, 581–594, doi:10.5194/amt-5-581-2012, 2012.

Clarisse, L., Coheur, P.-F., Prata, F., Hadji-Lazaro, J., Hurtmans, D., and Clerbaux, C.: A unified approach to infrared aerosol remote sensing and type specification, Atmos. Chem. Phys., 13, 2195–2221, doi:10.5194/acp-13-2195-2013, 2013.

Clerbaux, C., Coheur, P.-F., Clarisse, L., Hadji-Lazaro, J., Hurtmans, D., Turquety, S., Bowman, K., Worden, H., and Carn, S.: Measurements of SO_2 profiles in volcanic plumes from the NASA Tropospheric Emission Spectrometer (TES), Geophys. Res. Lett., 35, L22807, doi:10.1029/2008GL035566, 2008.

Clerbaux, C., Boynard, A., Clarisse, L., George, M., Hadji-Lazaro, J., Herbin, H., Hurtmans, D., Pommier, M., Razavi, A., Turquety, S., Wespes, C., and Coheur, P.-F.: Monitoring of atmospheric composition using the thermal infrared IASI/MetOp sounder, Atmos. Chem. Phys., 9, 6041–6054, doi:10.5194/acp-9-6041-2009, 2009.

Coheur, P.-F., Barret, B., Turquety, S., Hurtmans, D., Hadji-Lazaro, J., and Clerbaux, C.: Retrieval and characterisation of ozone vertical profiles from a thermal infrared nadir sounder, J. Geophys. Res., 110, D24303, doi:10.1029/2005JD005845, 2005.

Draxler, R. and Rolph, G.: HYSPLIT (HYbrid Single-Particle Lagrangian Integrated Trajectory) Model access via NOAA ARL READY Website, available at: http://www.arl.noaa.gov/HYSPLIT.php (last access date: 27 March 2014), 2013.

Fairlie, T. D., Vernier, J.-P., Natarajan, M., and Bedka, K. M.: Dispersion of the Nabro volcanic plume and its relation to the Asian summer monsoon, Atmos. Chem. Phys. Discuss., 13, 33177–33205, doi:10.5194/acpd-13-33177-2013, 2013.

Fromm, M., Nedoluha, G., and Charvát, Z.: Comment on "Large Volcanic Aerosol Load in the Stratosphere Linked to Asian Monsoon Transport", Science, 339, p. 647, doi:10.1126/science.1228605, 2013.

Hofmann, D., Barnes, J., O'Neill, M., Trudeau, M., and Neely, R.: Increase in background stratospheric aerosol observed with lidar at Mauna Loa Observatory and Boulder, Colorado, Geophys. Res. Lett., 36, L15808, doi:10.1029/2009GL039008, 2009.

Li, Q., Jiang, J. H., Wu, D. L., Read, W. G., Livesey, N. J., Waters, J. W., Zhang, Y., Wang, B., Filipiak, M. J., Davis, C. P., Turquety, S., Wu, S., Park, R. J., Yantosca, R. M., and Jacob, D. J.: Convective outflow of South Asian pollution: A global CTM simulation compared with EOS MLS observations, Geophys. Res. Lett., 32, L14826, doi:10.1029/2005GL022762, 2005.

Mateshvili, N., Fussen, D., Mateshvili, G., Mateshvili, I., Vanhellemont, F., Kyrölä, E., Tukiainen, S., Kujanpää, J., Bingen, C., Robert, C., Tétard, C., and Dekemper, E.: Nabro volcano aerosol in the stratosphere over Georgia, South Caucasus from ground-based spectrometry of twilight sky brightness, Atmos. Meas. Tech., 6, 2563–2576, doi:10.5194/amt-6-2563-2013, 2013.

Nowlan, C. R., Liu, X., Chance, K., Cai, Z., Kurosu, T. P., Lee, C., and Martin, R. V.: Retrievals of sulfur dioxide from the Global Ozone Monitoring Experiment 2 (GOME-2) using an optimal estimation approach: Algorithm and initial validation, J. Geophys. Res., 116, D18301, doi:10.1029/2011JD015808, 2011.

Park, M., Randel, W. J., Gettelman, A., Massie, S. T., and Jiang, J. H.: Transport above the Asian summer monsoon anticyclone inferred from Aura Microwave Limb Sounder tracers, J. Geophys. Res., 112, D16309, doi:10.1029/2006JD008294, 2007.

Park, M., Randel, W. J., Emmons, L. K., Bernath, P. F., Walker, K. A., and Boone, C. D.: Chemical isolation in the Asian monsoon anticyclone observed in Atmospheric Chemistry Experiment (ACE-FTS) data, Atmos. Chem. Phys., 8, 757–764, doi:10.5194/acp-8-757-2008, 2008.

Park, M., Randel, W. J., Emmons, L. K., and Livesey, N. J.: Transport pathways of carbon monoxide in the Asian summer monsoon diagnosed from Model of Ozone and Related Tracers (MOZART), J. Geophys. Res., 114, D08303, doi:10.1029/2008JD010621, 2009.

Pavolonis, M.: Development of a GOES-R Automated Volcanic Cloud Alert System, in: 2012 NOAA Satellite Science Week, available at: http://www.goes-r.gov/downloads/2012-Science-Week/pres/wed/pavolonis_volcanic-alerts.pdf, 2012.

Randel, W. J. and Park, M.: Deep convective influence on the Asian summer monsoon anticyclone and associated tracer variability observed with Atmospheric Infrared Sounder (AIRS), J. Geophys. Res., 111, D12314, doi:10.1029/2005JD006490, 2006.

Randel, W. J., Park, M., Emmons, L., Kinnison, D., Bernath, P., Walker, K. A., Boone, C., and Pumphrey, H.: Asian Monsoon Transport of Pollution to the Stratosphere, Science, 328, 611–613, doi:10.1126/science.1182274, 2010.

Robock, A.: Volcanic eruptions and climate., Rev. Geophys., 38, 191–219, doi:10.1029/1998RG000054, 2000.

Robock, A., Oman, L., and Stenchikov, G.: Regional climate responses to geoengineering with tropical and Arctic SO_2 injections, J. Geophys., 113, L15702, doi:10.1029/2007GL030524, 2007.

Rodgers, C.: Inverse methods for atmospheric sounding: theory and practice, series on atmospheric, oceanic and planetary physics, World Scientific, 2000.

SACS: Support to Aviation Control Service, available at: http://sacs.aeronomie.be/ (last access date: 27 March 2014), 2013.

Sawamura, P., Vernier, J., Barnes, J., Berkoff, T., Welton, E., Alados-Arboledas, L., Navas-Guzmán, F., Pappalardo, G. A., Mona, L., Madonna, F., Lange, D., Sicard, M., Godin-Beekmann, S., Payen, G., Wang, Z., Hu, S., Tripathi, S., Cordoba-Jabonero, C., and Hoff, R.: Stratospheric AOD after the 2011 eruption of Nabro volcano measured by lidars over the Northern Hemisphere, Environ. Res. Lett., 7, 034013, doi:10.1088/1748-9326/7/3/034013, 2012.

Solomon, S., Daniel, J. S., III, R. R. N., Vernier, J.-P., Dutton, E. G., and Thomason, L. W.: The Persistently Variable "Background" Stratospheric Aerosol Layer and Global Climate Change, Science, 333, 866–870, doi:10.1126/science.1206027, 2011.

Stenchikov, G. L., Kirchner, I., Robock, A., Graf, H.-F., Antuna, J. C., Grainger, R. G., Lambert, A., and Thomason, L.: Radiative forcing from the 1991 Mount Pinatubo volcanic eruption, J. Geophys. Res., 103, 13837–13857, doi:10.1029/98JD00693, 1998.

Theys, N., Campion, R., Clarisse, L., Brenot, H., van Gent, J., Dils, B., Corradini, S., Merucci, L., Coheur, P.-F., Van Roozendael, M., Hurtmans, D., Clerbaux, C., Tait, S., and Ferrucci, F.: Volcanic SO_2 fluxes derived from satellite data: a survey using OMI, GOME-2, IASI and MODIS, Atmos. Chem. Phys., 13, 5945–5968, doi:10.5194/acp-13-5945-2013, 2013.

Trenberth, K. and Dai, A.: Effects of Mount Pinatubo volcanic eruption on the hydrological cycle as an analog of geoengineering, Geophys. Res. Lett, 34, L15702, doi:10.1029/2007GL030524, 2007.

Uchino, O., Sakai, T., Nagai, T., Nakamae, K., Morino, I., Arai, K., Okumura, H., Takubo, S., Kawasaki, T., Mano, Y., Matsunaga,

T., and Yokota, T.: On recent (2008–2012) stratospheric aerosols observed by lidar over Japan, Atmos. Chem. Phys., 12, 11975–11984, doi:10.5194/acp-12-11975-2012, 2012.

Vernier, J.-P., Pommereau, J.-P., Thomason, L. W., Pelon, J., Garnier, A., Deshler, T., Jumelet, J., and Nielsen, J. K.: Overshooting of clean tropospheric air in the tropical lower stratosphere as seen by the CALIPSO lidar, Atmos. Chem. Phys., 11, 9683–9696, doi:10.5194/acp-11-9683-2011, 2011a.

Vernier, J.-P., Thomason, L. W., Pommereau, J.-P., Bourassa, A., Pelon, J., Garnier, A., Hauchecorne, A., Blanot, L., Trepte, C., Degenstein, D., and Vargas, F.: Major influence of tropical volcanic eruptions on the stratospheric aerosol layer during the last decade, Geophys. Res. Lett., 38, L12807, doi:10.1029/2011GL047563, 2011b.

Vernier, J.-P., Thomason, L. W., Fairlie, T. D., Minnis, P., Palikonda, R., and Bedka, K. M.: Comment on "Large Volcanic Aerosol Load in the Stratosphere Linked to Asian Monsoon Transport", Science, 339, p. 647, doi:10.1126/science.1227817, 2013.

von Clarmann, T., Grabowski, U., and Kiefer, M.: On the role of non-random errors in inverse problems in radiative transfer and other applications, J. Quant. Spectrosc. Ra., 71, 39–46, doi:10.1016/S0022-4073(01)00010-3, 2001.

Walker, J. C., Dudhia, A., and Carboni, E.: An effective method for the detection of trace species demonstrated using the MetOp Infrared Atmospheric Sounding Interferometer, Atmos. Meas. Tech., 4, 1567–1580, doi:10.5194/amt-4-1567-2011, 2011.

Walker, J. C., Carboni, E., Dudhia, A., and Grainger, R. G.: Improved detection of sulphur dioxide in volcanic plumes using satellite-based hyperspectral infrared measurements: Application to the Eyjafjallajökull 2010 eruption, J. Geophys. Res, 117, D00U16, doi:10.1029/2011JD016810, 2012.

Winker, D. M., Vaughan, M. A., Omar, A., Hu, Y., Powell, K. A., Liu, Z., Hunt, W. H., and Young, S. A.: Overview of the CALIPSO Mission and CALIOP Data Processing Algorithms, J. Atmos. Ocean. Tech., 26, 2310–2323, doi:10.1175/2009JTECHA1281.1, 2009.

Yang, K., Liu, X., Bhartia, P. K., Krotkov, N. A., Carn, S. A., Hughes, E. J., Krueger, A. J., Spurr, R. J. D., and Trahan, S. G.: Direct retrieval of sulfur dioxide amount and altitude from spaceborne hyperspectral UV measurements: Theory and application, J. Geophys. Res., 115, D00L09, doi:10.1029/2010JD013982, 2010.

Zarrin, A., Ghaemi, H., Azadi, M., Mofidi, A., and Mirzaei, E.: The effect of the Zagros Mountains on the formation and maintenance of the Iran Anticyclone using RegCM4, Meteorol. Atmos. Phys., 112, 91–100, doi:10.1007/s00703-011-0134-z, 2011.